Received: 19 January 2024 | Revised: 3 May 2024 | Accepted: 5 May 2024

DOI: 10.1002/glia.24542

GLIA

WILEY

RESEARCH ARTICLE

IL-10 and Cdc42 modulate astrocyte-mediated microglia activation in methamphetamine-induced neuroinflammation

Ana Isabel Silva[1,2,3] | Renato Socodato[4] | Carolina Pinto[1,2] | Ana Filipa Terceiro[1,2,3] | Teresa Canedo[1,2] | João Bettencourt Relvas[2,4,5] | Margarida Saraiva[2,6] | Teresa Summavielle[1,2,7]

[1]Addiction Biology Group, i3S-Instituto de Investigação e Inovação em Saúde, Porto, Portugal

[2]IBMC—Instituto de Biologia Molecular e Celular, Universidade do Porto, Porto, Portugal

[3]Instituto de Ciências Biomédicas de Abel Salazar (ICBAS), Universidade do Porto, Porto, Portugal

[4]Glia Cell Biology Group, i3S-Instituto de Investigação e Inovação em Saúde, Porto, Portugal

[5]Faculty of Medicine of the University of Porto (FMUP), Porto, Portugal

[6]Immune Regulation Group, i3S-Instituto de Investigação e Inovação em Saúde, Porto, Portugal

[7]ESS.PP, Escola Superior de Saúde do Politécnico do Porto, Porto, Portugal

Correspondence
Teresa Summavielle, Addiction Biology Group, i3S-Instituto de Investigação e Inovação em Saúde Porto, Portugal.
Email: tsummavi@i3s.up.pt

Funding information
Fundação para a Ciência e a Tecnologia, Grant/Award Numbers: PTDC/SAU-TOX/0067/2021, SFRH/BD/144324/2019, 2020.07188.BD, 2022.03699.CEECIND, CEECIND/00241/2017

Abstract

Methamphetamine (Meth) use is known to induce complex neuroinflammatory responses, particularly involving astrocytes and microglia. Building upon our previous research, which demonstrated that Meth stimulates astrocytes to release tumor necrosis factor (TNF) and glutamate, leading to microglial activation, this study investigates the role of the anti-inflammatory cytokine interleukin-10 (IL-10) in this process. Our findings reveal that the presence of recombinant IL-10 (rIL-10) counteracts Meth-induced excessive glutamate release in astrocyte cultures, which significantly reduces microglial activation. This reduction is associated with the modulation of astrocytic intracellular calcium (Ca^{2+}) dynamics, particularly by restricting the release of Ca^{2+} from the endoplasmic reticulum to the cytoplasm. Furthermore, we identify the small Rho GTPase Cdc42 as a crucial intermediary in the astrocyte-to-microglia communication pathway under Meth exposure. By employing a transgenic mouse model that overexpresses IL-10 (pMT-10), we also demonstrate in vivo that IL-10 prevents Meth-induced neuroinflammation. These findings not only enhance our understanding of Meth-related neuroinflammatory mechanisms, but also suggest IL-10 and Cdc42 as putative therapeutic targets for treating Meth-induced neuroinflammation.

KEYWORDS
cytokines, glia, Interleukin-10, psychostimulants, rho GTPase

1 | INTRODUCTION

Methamphetamine (Meth) is a highly addictive psychostimulant that poses significant public health challenges worldwide. Meth easily crosses the blood–brain barrier (BBB) (Xue et al., 2019), and exerts its effects through the exacerbation of monoaminergic and glutamatergic activities (Courtney & Ray, 2014; Panenka et al., 2013), causing long-term neuronal dysfunction and sustained behavioral consequences (Limanaqi et al., 2018). Meth is also well characterized as a powerful oxidative stress inducer (Yang et al., 2018). More recently, Meth was also shown to upregulate immune responses and cytokine production, culminating in pronounced neuroinflammation in which microglia activation is dependent on astrocytes (Canedo et al., 2021; Dang et al., 2021; Yang et al., 2018).

By demonstrating that astrocytes play such a central role in Meth-induced neuroinflammation, our finding shifts the focus of new therapies development from microglia to astrocytes, underscoring a crucial crosstalk between these two glial cell types. Beyond their immunocompetent roles, astrocytes contribute significantly to synapse formation, memory consolidation, and neurotransmitter regulation, including glutamate clearance

(Allen et al., 2012). Astrocytic glutamate signaling is intrinsically linked to drug-seeking behavior, as observed in cocaine addiction (Scofield et al., 2015). We previously reported that blocking glutamate receptors in microglia effectively prevents microglial activation by astrocytes exposed to Meth (Canedo et al., 2021). This evidence reinforces that glutamatergic signaling is a key player in modulating drug-seeking behavior (Tzschentke & Schmidt, 2003). Glutamate release can happen via both calcium (Ca^{2+})-dependent and independent mechanisms (Harada et al., 2015). Our prior studies have delineated Meth's ability to induce harmful glutamate release from astrocytes, fueling microglial reactivity in a tumor necrosis factor (TNF)- and Ca^{2+}-dependent manner (Canedo et al., 2021). We have shown that attenuating astrocytic Ca^{2+} release from the endoplasmic reticulum (ER) mitigates Meth's neuroinflammatory effects (Canedo et al., 2021).

A critical connection exists between glutamate, cytokines, and astrocyte-mediated microglial responses leading to neuroinflammation. In lipopolysaccharide (LPS)-stimulated microglia, the expression of the anti-inflammatory cytokine Interleukin (IL)-10 increases in response to excessive glutamate release (Werry et al., 2011), suggesting a complex interplay between neurotransmitters, cytokines, and neuroinflammatory responses. Reactive astrocytes can exacerbate microglial inflammatory responses through cytokines like TNF-α (Canedo et al., 2021), IL-6, GM-CSF, CCL2, and CXCL10 (Farina et al., 2007; Wheeler et al., 2019; Xu et al., 2017). In contrast, under IL-10 stimulation, astrocytes can nudge microglia toward anti-inflammatory states (Norden et al., 2014).

In rats, chronic administration of Meth, resulted in decreased circulating levels of IL-10, which were associated with reduced social interaction, increased anxiety, and impaired recognition memory (Swanepoel et al., 2018). Also in rats, overexpressing IL-10, specifically in the nucleus accumbens, reduced self-administration of the opioid remifentanil, though it was unclear which specific cell populations were responding to IL-10 (Lacagnina et al., 2017). Likewise, injecting recombinant IL-10 (rIL-10) into the basolateral amygdala attenuated binge-like ethanol consumption in mice (Marshall et al., 2017). Of note, epigenetic modifications in the IL-10-coding gene were correlated with addictive behaviors (Schwarz et al., 2011).

In this scenario, IL-10 exhibits a promising protective potential in Meth-induced neuroinflammation. Both microglia and astrocytes are capable of producing IL-10 and expressing its receptor, suggesting potential collaborative roles in neuroprotection (Burmeister & Marriott, 2018; Lobo-Silva et al., 2016). As such, in this work, we elucidate how IL-10 influences Meth-induced microglial activation by acting on astrocytes and demonstrate the protective effect of IL-10 on neuroinflammation caused by Meth.

2 | METHODS

2.1 | Animals

All experiments were conducted following the Directive 2010/63/EU and approved by the competent authorities Direção Geral de Alimentação e Veterinária (DGAV) and i3S Animal Ethical Committee (ref. 2018-13-TS and DGAV ref. 003891/2019-02-15). Researchers involved in animal experimentation were FELASA certified. All efforts were made to minimize animal suffering and the number of animals used. Mice were housed under specific pathogen-free conditions in a controlled environment (20°C, 45%–55% humidity) with an inverted 12 h/12 h light/ dark cycle and free access to food and water. The pMT-10 mouse was generated by inserting a construct containing the IL-10 cDNA under the control of the inducible sheep metallothionein (MT) promoter in the genome of wild-type (WT) BL/6 mice. The MT promoter is activated in the presence of 50 mM of Zn in the organism, administered in the drinking water. For details on the construct and/or kinetics of IL-10 expression upon Zn administration please see (Cardoso et al., 2018). The pMT-10.IL-10Ra$^{-/-}$ (Cardoso et al., 2018) mouse was generated by crossing pMT-10 (Mesquita et al., 2008) and IL-10Ra$^{-/-}$ (Pils et al., 2010) mice. These mice respond to Zn by upregulating IL-10, but do not subsequently respond to IL-10 due to lack of the IL-10R alpha chain (Cardoso et al., 2021). pMT-10 and pMT-10.RIL-10Rα$^{-/-}$ mice were bred at i3S under specific pathogen-free conditions.

2.2 | IL-10 induction

IL-10 overexpression was induced via administering Zn sulfate heptahydrate ($ZnSO_4.7H_2O$) in the drinking water, as reported (Cardoso et al., 2018). A solution of 50 nM Zn with 2% sucrose was fed to the mice ad libitum during the experimental period.

2.3 | Meth administration to mice

Mice were subjected to a Meth binge protocol (Canedo et al., 2021) and randomly assigned to the Meth group (4 × 5 mg/kg Meth, 2 h apart, intraperitoneally) or the control group (4× isovolumetric saline) and sacrificed 24 h after the first administration. Meth hydrochloride was imported from Sigma-Aldrich (MO, USA) under a special INFARMED license.

2.4 | Microglial quantification and morphometric analysis

Mice were anesthetized and perfused with PBS. Brains were post-fixed for 48 h in 4% paraformaldehyde (PFA), cryoprotected using a 30% sucrose gradient, embedded in OCT, frozen, and cryosectioned (coronally at 30 µm, between Bregma positions 1.0–2.0 mm) in the CM3050S cryostat (Leica Biosystems, Wetzlar, DE). Brain sections were collected and stored at 4°C until further use. Brain slices (free-floating) were selected and permeabilized with 0.2% Triton X-100 and 10% fetal bovine serum (FBS) in PBS (blocking solution) for 1 h at room temperature (RT) as in (Canedo et al., 2021). Then, brain sections were incubated with primary antibody Iba-1 (1:500, Wako) (4°C) in a blocking solution for 72 h under agitation. After washing, sections

were incubated with a secondary antibody diluted in blocking solution (1:1000, Invitrogen) conjugated to Alexa Fluor for 24 h (4°C) with agitation, and nuclei were stained with DAPI. After PBS washes, sections were mounted using Fluoroshield (Sigma-Aldrich) and visualized in a TCS SP5 II confocal microscope (Leica Biosystems). For microglial cell quantification, images were acquired using a Leica HCX PL APO 40× water-immersion lens with a z-step size of 0.33 mm. Iba-1+ cells were counted manually using Fiji software with Z-stack projection images. For morphometric analysis, images were acquired using a Leica HCX PL APO 63X 1.3 glycerol-immersion lens with 4.5× digital zoom and a z-step size of 0.33 mm. Microglia 3D reconstructions were performed using the IMARIS software (version 10.0, Bitplane, Belfast, UK).

2.5 | Astrocytic morphometric analysis

Brain slices (free-floating) were selected and permeabilized with 0.2% Triton X-100 10% FBS in PBS (blocking solution) for 1 h at RT. Then, brain sections were incubated with primary antibody GFAP (1:500, Abcam) (4°C) in blocking solution for 72 h under agitation, a marker for mature astrocytes in the CNS, as previously described (Althammer et al., 2020; SheikhBahaei et al., 2018). After washing, sections were incubated with secondary antibodies diluted in blocking solution (1:1000, Invitrogen) conjugated to Alexa Fluor for 24 h (4°C) with agitation. After PBS washes, sections were mounted using Fluoroshield (Sigma-Aldrich) and visualized in a TCS SP5 II confocal microscope (Leica Biosystems). Images were acquired using a Leica HCX PL APO 63X 1.3 glycerol-immersion lens with 3× digital zoom and a z-step size of 0.33 mm. Astrocytes 3D reconstructions were performed using the IMARIS software (version 10.1.0, Bitplane, Belfast, UK).

2.6 | In vivo synapse engulfment quantification

Brain slices (free-floating) were selected and permeabilized with 0.2% Triton X-100 10% FBS in PBS (blocking solution) for 1 h at RT. Then, brain sections were incubated with primary antibodies Iba-1 (1:500, Wako), CD68 (1:500, Bio-Rad), and PSD-95 (1:500, Cell Signaling) (4°C) in blocking solution for 72 h under agitation. After washing, sections were incubated with secondary antibodies diluted in blocking solution (1:1000, Invitrogen) conjugated to Alexa Fluor for 24 h (4°C) with agitation. After PBS washes, sections were mounted using Fluoroshield (Sigma-Aldrich) and visualized in a TCS SP5 II confocal microscope (Leica Biosystems). Images were acquired using a Leica HCX PL APO 63× 1.3 glycerol-immersion lens with 4.5× digital zoom and a z-step size of 0.33 mm. Images were processed and analyzed by Imaris Software (Bitplane, Switzerland). CD68 and Iba-1 volumes were quantified by applying 3D surface rendering of confocal stacks in their respective channels, using identical settings (fixed thresholds of intensity and voxel) within each experiment. For quantification of PSD95 engulfment by microglia, only PSD95 puncta present within microglial CD68 structures were considered. This procedure ensured that only puncta entirely phagocytosed by microglia were included in the analysis. To this aim, a new channel for "engulfed PSD95" was created using the mask function in Imaris, masking the PSD95 signal within CD68+ structures. Quantification of volumes for "engulfed PSD95 in CD68" was performed following the "3D Surface rendering of engulfed material" protocol, previously published by (Schafer et al., 2014). To account for variations in cell size, the amount of "engulfed PSD95 in CD68" was normalized to the total volume of the phagocyte (given by Iba-1 total volume).

2.7 | Elevated plus maze

As we previously described, anxiety-like behavior was assessed using the elevated plus maze (EPM) test (Canedo et al., 2021; Socodato et al., 2020). The test was performed 24 h after the first Meth administration, just before the euthanasia. The test was conducted in the dark phase of the light/dark cycle. The maze, made of opaque gray polyvinyl, consisted of four arms arranged in a cross-shape; two closed arms have surrounding walls (18 cm high), opposing two open arms (all arms 37 × 6 cm). The apparatus was elevated at a height of 50 cm. Each mouse was placed on the central platform facing an open arm and allowed to explore the maze for 5 min. The mice's movement and location were recorded and analyzed by Smart Video Tracking Software v 2.5 (Panlab, Harvard Apparatus).

2.8 | Primary cell cultures

Primary mixed glial cultures were performed as previously described (Canedo et al., 2021). Briefly, neonatal Wistar rats were sacrificed. The cortex, embedded in Hank's balanced salt solution (HBSS) (Gibco™, 14170112) + 1% of PenStrep (Gibco™, 15140122), was placed on ice. Mechanical digestion was performed until the mixture looked homogeneous. Afterward, enzymatic digestion was completed using DNase I and Trypsin–EDTA (0.25%) (Gibco™,25200072). The culture medium, DMEM GlutaMAX™ (Gibco™, 10566016) with 10% FBS, was added to inactive trypsin, and then the mixture was centrifuged, and the pellet was resuspended in the culture medium. Cells were seeded in T75 flasks with supplemented DMEM GlutaMAX™-I, constituted by 10% fetal bovine serum (FBS from Gibco™, 10270106) Heat Inactivated, Gentamicin (120 µg/mL; BioWhittakerTM), and Amphotericin B (0.25 µg/mL; Sigma-Aldrich). Cells were maintained at an appropriate temperature and gas mixture (37°C and 5% CO_2). After 10 days in vitro, these cell cultures should be free of neurons, meningeal cells, and fibroblasts and composed only of astrocytes, oligodendrocytes, and microglia (de Vellis & Cole, 2012).

Flasks were shaken for 2 h at 200 rpm at 37°C to obtain purified microglia cultures. The medium from the flasks was collected and centrifuged at 1200 rpm for 10 min. The supernatant was discarded, and the pellet was suspended in warm supplemented DMEM-F12 GlutaMAX™ (Gibco™, 10565018). The number of live cells was determined by gently mixing the cell mixture with trypan blue solution 0.4% (Gibco™, 15250061). The cell suspension was then diluted in warm-

supplemented DMEM-F12 GlutaMAX™. Cells were seeded and placed in the incubator for 2 days. Immunolabeling with CD11b and Hoechst showed a purity of 97% for these cultures (Figure S1A).

For purified astrocytic cells, flasks were placed in an orbital shaker (overnight at 220 rpm at 37°C) to remove non-astrocytic cells. Next, astrocytes were detached and split into non-coated T-flasks in DMEM GlutaMAX™. Split cultures were re-split at least four times to obtain purified cultures. Primary cultures of astrocytes were used between passages 5 and 7. Immunolabeling with GFAP and Hoechst showed a purity of 86% for these cultures (Figure S1A).

2.8.1 | Cell treatments

Astrocytes were treated to create an astrocytic conditioned medium (ACM) as before (Canedo et al., 2021). Briefly, primary cell cultures of astrocytes were seeded and incubated until confluence (~80%) was reached. At that moment, cells were treated with cell culture medium and 0, 5, 10, or 20 ng/mL of recombinant IL-10 (rIL-10) (CT+rIL-10) or with 100 μM of Meth and 0, 5, 10, or 20 ng/mL of rIL-10 (Meth +rIL-10) for 24 h. After this time, the conditioned medium (ACM CT +rIL-10 or ACM Meth+rIL-10) was collected, centrifuged for debris removal (1200 rpm, 5 min), and frozen at −80°C until used. To assess the effects of ACM on purified primary microglial cultures, microglial cells were exposed to ACM CT+rIL-10 or ACM Meth+rIL-10 for 24 h in the same concentrations described above. The rat rIL-10 (Cys167Try) Protein was purchased from R&D Systems.

2.8.2 | Immunocytochemistry

Primary cell cultures of microglia, plated in a 96-well plate, were fixated with 4% PFA (Sigma-Aldrich) for 10 min at RT. Then, cells were permeabilized with 0.1% Triton X-100 (Sigma-Aldrich) for 10 min at RT and blocked with 3% bovine serum albumin (BSA; Sigma-Aldrich) for 1 h at RT. Fixed cells were incubated with primary antibodies iNOS (1:200, abcam) and CD68 (1:500, biorad) overnight at 4°C.

Cells were incubated with secondary antibodies (1:1000, Invitrogen), conjugated to Alexa Fluor, for 1 h at RT, and nuclei stained with 0,5 μg/mL Hoechst 33342 (Sigma-Aldrich) and HCS Cell Mask (Invitrogen; 0.5 μg/mL) for 30 min at RT. Finally, cells were rewashed with PBS1× and visualized at IN Cell Analyzer 2000 at an objective of 40×. The signal intensity was then quantified using Cell Profiler 4.2.

2.8.3 | Plasmids

Cells transfection was performed using 1–2 μg of each plasmid with jetPRIME (Polyplus transfection, Illkirch-Graffenstaden, France) according to the manufacturer's protocol.

The glutamate release from astrocytes were measured using pDisplay FLIPE-600n (Addgene #13545) (Okumoto et al., 2005). The efflux of Ca^{2+} from the ER into the cytosol of microglia was measured using the D1ER biosensor (Addgene #36325) (Palmer et al., 2004). The specific activity of c-Src at the plasma membrane of microglia was measured using the Lyn Src (WT) YPet FRET probe (here mentioned as Src biosensor) (Addgene #78302) (Wang et al., 2005).

Raichu RhoA, Raichu-Rac1, and Raichu-Cdc42 were provided by M. Matsuda (Yoshizaki et al., 2003).

2.8.4 | FRET-based live cell assay

Primary astrocytes were plated on plastic-bottom culture dishes (μ-Dish 35 mm, iBidi) at a concentration of 1 × 105 cells/mL with an extra 1 mL of supplemented DMEM GlutaMAX™. The plate was incubated for 24 h, and after that period, the transfection mix was prepared and added to the cells according to the manufacturer's instructions. Briefly, the transfection mixture contained the desired DNA, JetPrime Buffer, and the JetPrime Reagent. The cells were incubated again for 48 h, washed with HBSS, and incubated with 1 mL of HBSS for 30 min. During this time, the stimulus for the cells was prepared. Three different stimuli were diluted in HBSS. Imaging was performed using a Leica DMI6000B inverted microscope as previously described (Socodato et al., 2015; Socodato et al., 2018). The excitation light source was a mercury metal halide bulb integrated with an EL6000 light attenuator. High-speed, low-vibration external excitation/emission filter wheels equipped with filter cubes for cyan fluorescent protein (CFP) (BP 427/10) and yellow fluorescent protein (YFP) (BP 504/12) working with specific dichroic (CG1 440/520) and a separate filter cube for monomeric red fluorescent protein (mRFP) (ex. BP580/20; DM 595; em. 630/55) mounted into a microscope filter carrousel (Leica fast filter wheels) and a PlanApo 63× 1.3NA glycerol immersion objective were used for CFP and FRET images. Images were acquired with 2 × 2 binning using a digital CMOS camera (ORCAFlash4.0 V2, Hamamatsu Photonics). Images were exported as 16-bit tiff files and processed in FIJI software. The background was dynamically subtracted from all slices from both channels. Segmentation was achieved on a pixel-by-pixel basis using a modification of the Huang algorithm. After background subtraction and filtering, ratiometric images (CFP/FRET or FRET/CFP) were generated in intensity-modulated display mode using the FRET images as intensity modulators.

2.8.5 | FRET-based fixed cell assay

Primary astrocytes were seeded onto PhenoPlate96 (6055302, Revvity) microplates at a density of 6 × 10^4 cells/mL in supplemented DMEM GlutaMAX™. Following a 24-h incubation, a transfection mix was prepared and applied to the cells per the manufacturer's guidelines. The transfection mixture included the desired DNA, JetPrime Buffer, and JetPrime Reagent. Subsequently, cells were fixed with 4% PFA for 10 min at RT. Automated image acquisition was conducted using an Opera Phenix® Plus high-content screening (HCS) system (Revvity) in confocal mode, and image analysis was carried out using Harmony® high-content analysis software (Revvity). Initially, low-magnification (10×/0.3 NA Air) whole-well imaging of the YFP channel (ex. 488, em. 500–550)

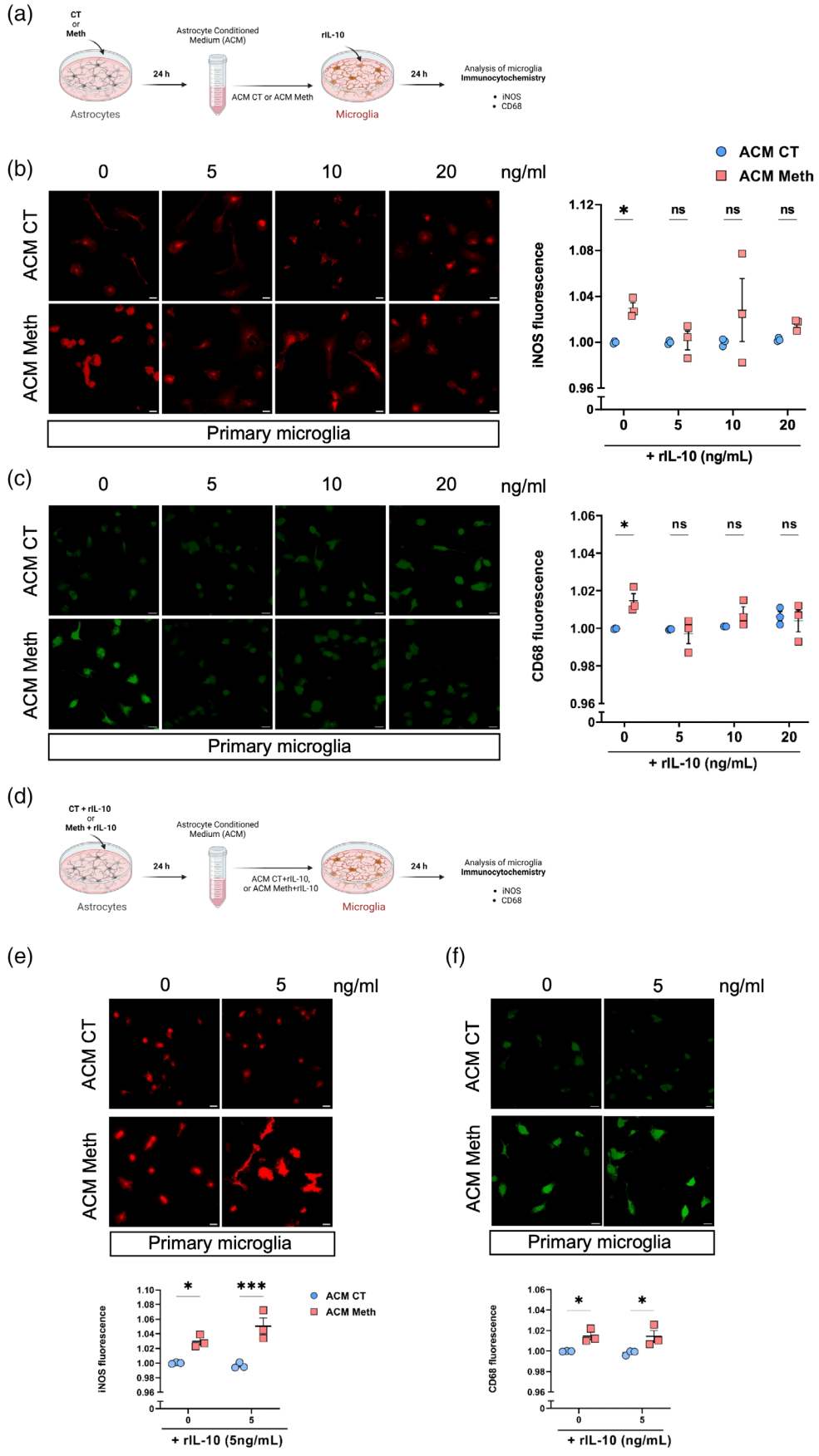

FIGURE 1 Legend on next page.

was performed to identify transfected cells, which were then recaptured at high magnification (63×/1.1 NA Water) in the Cerulean channel (ex. 405, em. 435–480) and YFP channel (ex. 405, em. 500–550) across a z-section of 3 μm (7 × 0.5 μm). The acquired stacks underwent maximum projection, and the FRET ratio (mean fluorescent intensity ratio of Cerulean/YFP or YFP/Cerulean) was subsequently determined.

2.9 | Statistical analysis

Results were expressed as mean ± standard error of the mean (SEM). When comparing only two experimental groups, the paired Student *t*-test with equal variance assumption was used for data with normal distribution. A one-way analysis of variance (ANOVA) without repeated measures was performed when comparing three or more groups. A 95% confidence interval and statistical significance were set at $p < .05$. All quantifications were performed blindly. Analysis was achieved using the GraphPad Prism® software version 9.3.1 for windows. The terminology used in graphics reads as follows: ****$p < .0001$; ***$p < .001$; **$p < .01$, *$p < .05$. $p > .05$ was considered to indicate no significance and is denoted by "ns."

3 | RESULTS

3.1 | IL-10 modulates astrocytic responses, preventing Meth-induced microglia activation

We previously established that binge administration of Meth induces microgliosis in vivo (Canedo et al., 2021). Notably, in vitro activation of microglial cells did not result from direct Meth action but instead from pro-inflammatory soluble factors produced by astrocytes in response to Meth (Canedo et al., 2021). Given the anti-inflammatory properties of IL-10, we questioned whether the presence of this cytokine would reduce Meth-induced astrocyte-mediated microglial activation. To investigate that, we used primary cell cultures. We prepared astrocyte conditioned medium (ACM) obtained from astrocytes exposed to Meth, spiked with a range of recombinant IL-10 (rIL-10) concentrations (ACM Meth+rIL-10) (Lim et al., 2013). ACM obtained from astrocytes that were not exposed to Meth with correspondent concentrations of rIL-10 (ACM CT+rIL-10) were used as controls. Meth exposure and ranging levels of rIL-10 did not affect the viability of astrocytic cell cultures (Figure S1B). Microglia cultures were then exposed to these different ACM and microglia activation was analyzed 24 h later (Figure 1a). We found that the addition of rIL-10 (5 and 20 ng/mL) to astrocytes significantly prevented the increase in iNOS levels in microglia caused by ACM Meth alone (Figure 1b). Because activated microglia increase phagocytic activity markers, we further investigated if rIL-10 interfered with the increase in microglial CD68 expression that we previously reported in mice exposed to Meth (Canedo et al., 2021). We found that rIL-10 in astrocytes efficiently prevented the increase of CD68 in microglia triggered by ACM Meth (Figure 1c). These results suggest that IL-10 counteracts the stimulatory effect of Meth.

Next, we investigated whether the effects of rIL-10 occurred via astrocytes or were directly exerted on microglia. For that, microglia cells were exposed to ACM Meth, and IL-10 was added directly to the microglia cultures (Figure 1d). The concentration of rIL-10 chosen for direct microglial exposure was 5 ng/mL, the lowest concentration previously demonstrated to be effective when added to astrocytes. Of note, rIL-10 did not exert a direct protective effect on microglia activation regarding iNOS activity (Figure 1e) or CD68 expression (Figure 1f). This suggests that the inhibitory effect of IL-10 primarily occurs through its action on astrocytes, possibly implying that IL-10 leads to alterations in the ACM composition.

FIGURE 1 IL-10 modulates astrocytic response and prevents Meth-induced microglia activation. (a) Experimental design—primary astrocytic cell cultures were incubated with 0, 5, 10, or 20 ng/mL of rIL-10 (CT+rIL-10) or 100 μM Meth and 0, 5, 10, or 20 ng/mL of rIL-10 (Meth+rIL-10) for 24 h. Following that, primary microglial cultures were incubated with the conditioned medium obtained from the astrocytes maintained solely with rIL-10 (ACM CT+rIL-10) or Meth plus rIL-10 (ACM Meth+rIL-10) for 24 h. After this, microglia reactivity markers such as iNOS and CD68 were analyzed by immunohistochemistry. Created with BioRender.com. (b) Fluorescence representative images of immunolabeling for iNOS (red) in primary microglia exposed to ACM CT+rIL-10 or ACM Meth+rIL-10 ($n = 3$ independent cultures). Scale bar, 20 μm. Data were normalized to the value of control (ACM CT+rIL-10) for each concentration of rIL-10. Symbols represent mean values for each independent cell culture, and error bars represent the standard error of the mean (SEM). Statistical analysis was conducted using a two-way analysis of variance (ANOVA) with multiple comparisons (*$p < .05$, **$p < .01$, and ns, non-significant). (c) Fluorescence representative images of immunolabeling for CD68 (green) in primary microglia exposed to ACM CT+rIL-10 or ACM Meth+rIL-10 ($n = 3$ independent cultures). Scale bar, 20 μm. Data was normalized to the value of control (ACM CT+rIL-10) for each concentration of rIL-10. Symbols represent the mean value of each independent cell culture ± SEM. Statistical analysis was conducted using a two-way ANOVA with multiple comparisons (*$p < .05$ and ns, non-significant). (d) Experimental design—primary astrocytic cell cultures were incubated with cell culture medium (CT) or 100 μM Meth for 24 h. Following that, primary microglial cultures were incubated with rIL-10 and the conditioned medium obtained from astrocytes, ACM CT or ACM Meth, for 24 h. After this, microglia reactivity markers such as iNOS and CD68 were analyzed by immunohistochemistry. Created with BioRender.com. (e) Fluorescence representative images of immunolabeling for iNOS (red) in primary microglia exposed to ACM CT plus rIL-10 or ACM Meth plus rIL-10 ($n = 3$ independent cultures). Scale bar, 20 μm. Data was normalized to the value of control (ACM CT+rIL-10) for each concentration of rIL-10. Symbols represent the mean value of each independent cell culture ± SEM. Statistical analysis was conducted using an unpaired *t*-test, (*$p < .05$, ***$p < .001$). (F) Fluorescence representative images of immunolabeling for CD68 (green) in primary microglia exposed to ACM CT and rIL-10 or ACM Meth and rIL-10 ($n = 3$ independent cultures). Scale bar, 20 μm. Data were normalized to the value of control (ACM CT plus rIL-10) for each concentration of rIL-10. Symbols represent the mean value of each independent cell culture ± SEM. Statistical analysis was conducted using an unpaired *t*-test (*$p < .05$).

3.2 | IL-10 inhibits Meth-induced astrocytic glutamate release

Meth induces a rapid and significant release of glutamate from astrocytes, which was implicated in subsequent microglia activation (Canedo et al., 2021). Thus, we hypothesized that rIL-10 could exert its inhibitory effect by reducing glutamate release from astrocytes. We tested this hypothesis using the glutamate release FRET biosensor FLIPE 600n^{SURFACE} (Okumoto et al., 2005) to monitor, in real-time, the release of glutamate from astrocytes exposed to Meth in the presence or absence of 5 ng/mL rIL-10. In accordance with what was previously described (Canedo et al., 2021), Meth triggered a rapid and sustained release of glutamate from astrocytes (Figure 2a). Incubation of astrocytes with rIL-10 significantly reduced the glutamate release triggered by Meth. In contrast, exposure to rIL-10 alone had no effect in glutamate release (Figure 2a).

3.3 | IL-10 modulates astrocytic calcium signaling and Cdc42 activation triggered by Meth

Astrocytes can release glutamate from intracellular pools through various mechanisms, including Ca^{2+}-dependent and -independent pathways (Harada et al., 2015). We have established that an increased efflux of Ca^{2+} from the ER pool to the cytosol is required for the astrocytic glutamate release triggered by Meth (Canedo et al., 2021). Thus, we hypothesized that IL-10 might mitigate glutamate release by influencing the release of Ca^{2+} from the ER. To verify this, we utilized the D1ER FRET biosensor (Palmer et al., 2004) to detect the efflux of Ca^{2+} from the ER into the cytosol in astrocytes exposed to Meth. Confirming previous results (Canedo et al., 2021), Meth caused the release of Ca^{2+} from the ER to the cytosol (Figure 2b), while the presence of rIL-10 led to a significant reduction of Meth-induced Ca^{2+} efflux, indicating an IL-10 exerted modulatory effect (Figure 2b). Additionally, rIL-10 alone led to increased Ca^{2+} efflux from the ER (Figure 2b).

We next investigated the molecular players underlying the effect of IL-10 in regulating Meth-induced Ca^{2+} release. Since Ca^{2+} signaling has been associated with the activity of Src-family tyrosine kinases (SFKs) (Anguita & Villalobo, 2017; Giusti et al., 1999; Minuz et al., 2018), we hypothesized that IL-10 could mediate calcium release by acting on c-Src activity. First, we examined whether Meth alone activated c-Src in astrocytes. Using a specific c-Src FRET-based biosensor (KRas Src YPet) that does not recognize the activity of other SFKs (Ouyang et al., 2008), we observed that Meth did not significantly affect c-Src activity in astrocytes, as evidenced by the lack of changes in the Donor/FRET emission ratio of the KRas Src YPet probe (Figure S2A). In face of these results, we concluded that Src-family is not downstream of IL-10 signaling in astrocytes.

We then addressed the involvement of the small Rho GTPases family, specifically Cdc42, Rac1, and RhoA, which are well-known regulators of cell dynamics in response to psychostimulants and of intracellular Ca^{2+} levels (Aspenström, 2004; Ding et al., 2022; Inaba et al., 2021; Narita et al., 2003), as well as of other processes known to be involved in glutamate release from astrocytes (Malarkey & Parpura, 2008). Although the impact of Meth on Rho GTPases has been documented (Ru et al., 2023), its specific effects on astrocytes remained uncharacterized. Using FRET-based biosensors in primary astrocytes, we found that Meth induced a rapid and sustained increase in astrocytic Cdc42 activity (Figure 2c). Importantly, IL-10 significantly prevented this Meth-induced increase in Cdc42 activation, while having no impact on Cdc42 activity on its own (Figure 2c). Further kinetic analyses showed that Meth had no significant effect on Rac1 activity (Figure S2B), suggesting that this molecule is not involved in IL-10-action in Meth-exposed astrocytes. Analysis of the RhoA activity under Meth exposure revealed a significant increase between the first 5–15 min (Figure S2C). Although rIL-10 partially prevented the Meth-induced increase in RhoA activity, rIL-10 on its own also promoted a sustained increased in RhoA activity (Figure S2C). Taken together, the Rho GTPase kinetics data prompted us to conclude that Cdc42 was most likely the Rho GTPase involved in relaying the inhibitory effects of IL-10 on astrocytes exposed to Meth.

3.4 | Cdc42 inhibition is sufficient to prevent astrocytic glutamate release but not Ca^{2+} signaling

The above findings suggest that IL-10 counteracts the effects of Meth in astrocytes (and consequently on microglia) by interfering with Cdc42 activity, which in itself mediates Meth-activation of astrocytes. Next, we questioned whether blocking this Rho GTPase with a pharmacological inhibitor would impact the effect of Meth in astrocytes. For that, we inhibited Cdc42 using Zcl278, a Cdc42-specificfic inhibitor that targets the interaction between Intersectin1-long (Itsn1-L) and Cdc42 (Friesland et al., 2013). Zcl278 was previously shown not to have adverse effects on cell viability (An et al., 2016; Liu et al., 2015). Zcl278 effectively prevented Meth-induced activation of Cdc42 in astrocytic cultures, whereas, as expected, Zcl278 alone decreased Cdc42 activation (Figure 3a).

To clarify if Meth-induced Cdc42 activation was involved in astrocytic glutamate release, we inhibited Cdc42 and evaluated whether this could prevent the release of glutamate. We observed that treatment with Zcl278 led to a significant reduction in the Meth-induced glutamate release from astrocytes (Figure 3b). Together with the IL-10 data, this strongly suggests that, in astrocytes, Meth-induced glutamate release is dependent on the activation of Cdc42.

Cdc42, alongside other Rho GTPases, is recognized for its role in orchestrating intracellular Ca^{2+} dynamics (Aspenström, 2004; Costello et al., 1999; Djouder et al., 2000). Specifically, Cdc42 has been described to activate Ca^{2+} signaling pathways, thereby facilitating the exocytosis of secretory granules (Hong-Geller & Cerione, 2000). Thus, we next investigated whether Meth-induced Ca^{2+} release from the ER depended on Cdc42 activation. Inhibition of Cdc42 by Zcl278 did not affect Ca^{2+} release in a significant way (Figure 3c and Figure S2D). Based on these data, we concluded that IL-10 protective action on

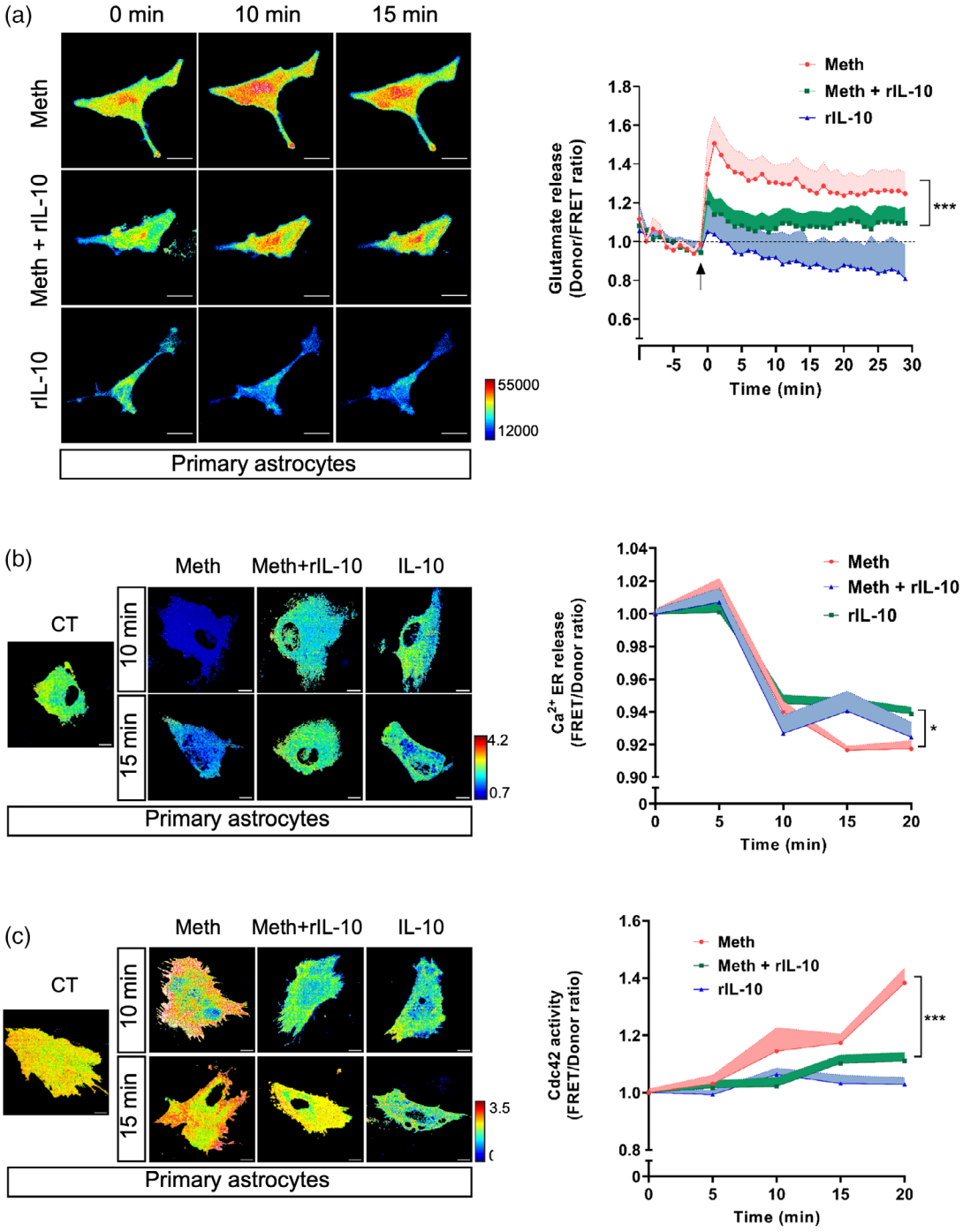

FIGURE 2 IL-10 inhibits Meth-induced astrocytic glutamate release preventing Ca^{2+} efflux and Cdc42 increased activity. (a)Primary astrocytes expressing the glutamate release FRET biosensor (FLIPE) were incubated in control medium (CT), and exposed to 100 μM Meth, Meth +rIL-10 (5 ng/mL) or IL-10 (5 ng/mL) alone. The time-lapse Donor/FRET ratio changes for the FLIPE biosensor (normalized at 0 min) were color-coded according to the scale. Scale bars 20 μm. Data were based on $n = 9$ to 11 cells, pooled across 4 independent experiments. Symbols represent mean values + standard error of the mean (SEM). The arrow indicates the time point in which treatments were administered. A two-way analysis of variance (ANOVA) was performed to evaluate the interaction between the treatment and the time-points (***$p < .001$). (b) Primary astrocytes expressing the endoplasmic reticulum calcium release FRET biosensor (D1ER) were incubated in CT and exposed to 100 μM Meth, Meth+rIL-10 (5 ng/mL) or IL-10 (5 ng/mL) alone for 5, 10, 15, or 20 min. FRET/Donor ratio changes for the D1ER biosensor (normalized to control cells) are shown according to the scale. Scale bar, 50 μm. Symbols represent mean values + SEM of $n = 550$ to 598 cells pooled across three independent experiments. A two-way ANOVA was performed to evaluate the interaction between treatment and time-points (*$p < .05$). (c) Primary astrocytes expressing Raichu-Cdc42 biosensor were incubated in CT and exposed to 100 μM Meth, Meth+rIL-10 (5 ng/mL) or IL-10 (5 ng/mL) alone for 5, 10, 15, or 20 min. FRET/Donor ratio changes for the Raichu-Cdc42 biosensor (normalized to control cells) are shown according to the scale. Scale bar, 50 μm. Symbols represent mean values + SEM for $n = 550$ to 598 cells pooled across 3 independent experiments. A two-way ANOVA was performed to evaluate the interaction between the treatment and the time-points (***$p < .001$).

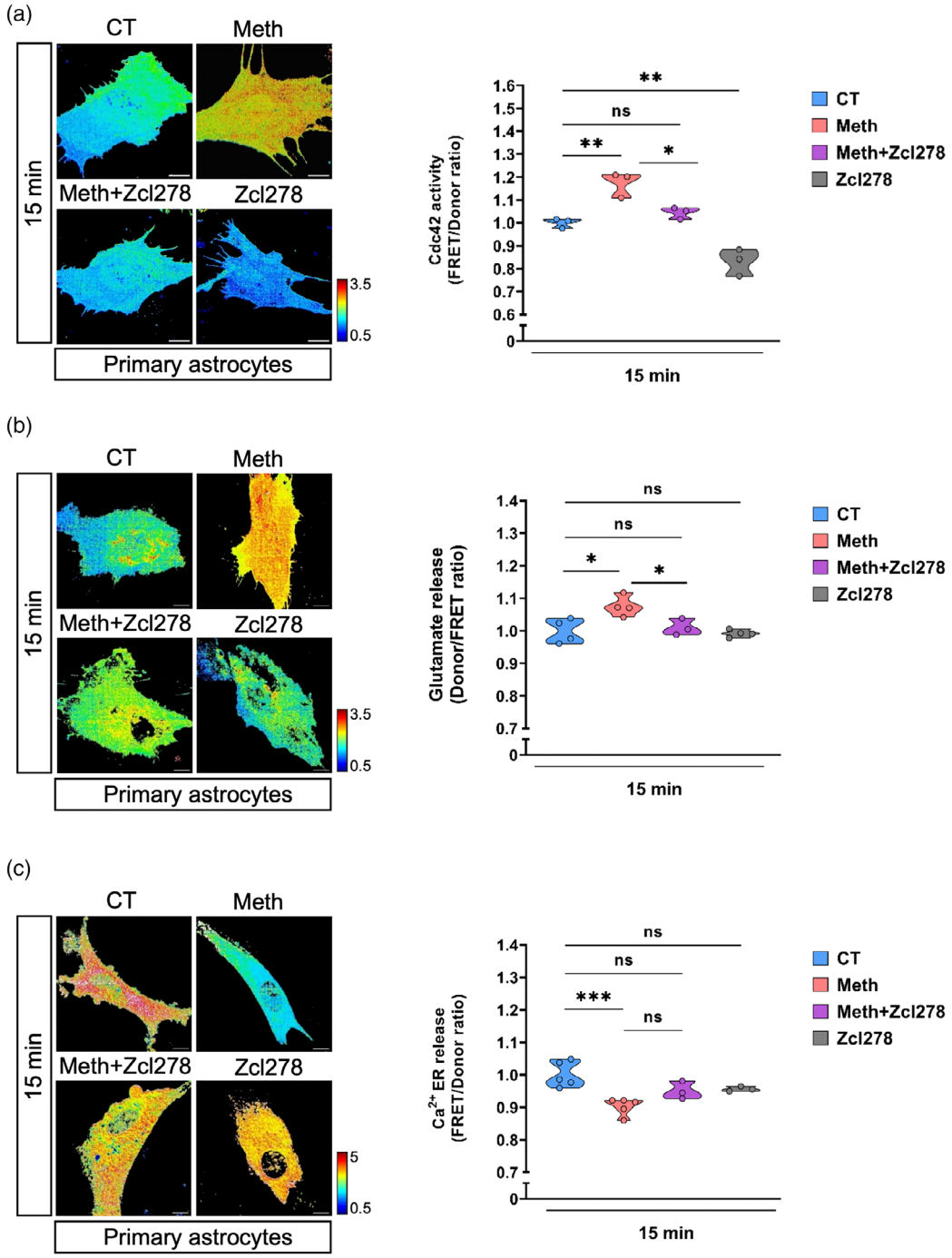

FIGURE 3 Cdc42 inhibition is sufficient to prevent glutamate release from astrocytes. (a) Primary astrocytes expressing Raichu-Cdc42 biosensor were incubated in control medium (CT) and exposed to 100 μM Meth, Meth+Zcl278 (50 μM), or Zcl278 (50 μM). FRET/Donor ratio changes for the Raichu-Cdc42 biosensor (normalized to control cells) were evaluated at 15 min and are shown according to the scale. Scale bar, 50 μm. Symbols represent mean values ± standard error of the mean (SEM) of $n = 18$ to 50 cells from 3 independent experiments. Statistical analysis was conducted using a two-way analysis of variance (ANOVA) with multiple comparisons (*$p < .05$, **$p < .01$, and ns, non-significant). (b) Primary astrocytes expressing the glutamate release FRET biosensor (FLIPE) were incubated in CT, and exposed to 100 μM Meth, Meth +Zcl278 (5,0 μM) or Zcl278 (50 μM). Donor/FRET ratio changes (normalized for control cells) were evaluated at 15 min and are shown according to the scale. Scale bar, 50 μm. Symbols represent mean values ± SEM, for $n = 379$ to 412 cells from 3 to 4 independent experiments. Statistical analysis was conducted using two-way ANOVA with multiple comparisons (*$p < .05$, and ns, non-significant). (c) Primary astrocytes expressing the endoplasmic reticulum calcium release FRET biosensor (D1ER) were incubated in CT, and exposed to 100 μM Meth, Meth+Zcl278 (5,0 μM) or Zcl278 (50 μM). Donor/FRET ratio changes (normalized for control cells) were evaluated at 15 min and are shown according to the scale. Scale bar, 50 μm. Symbols represent mean values ± SEM, for $n = 50$ to 599 cells pooled across 3–5 independent experiments. A two-way ANOVA was performed to evaluate the interaction between the treatment and the time-points, (***$p < .001$, and ns, non-significant).

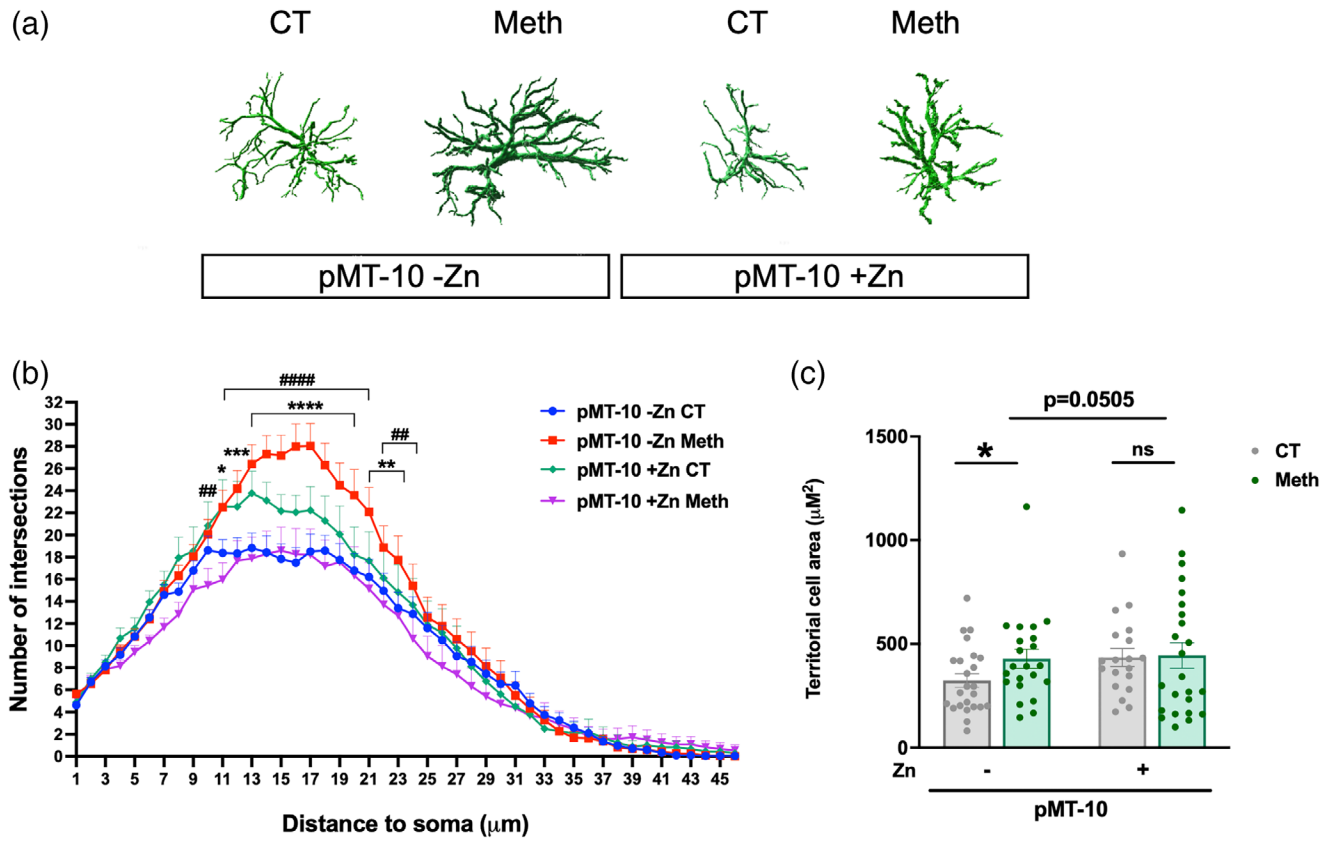

FIGURE 4 Meth causes astrocyte morphological alterations and IL-10 is sufficient to counteract them. (a) Imaris (Bitplane)-based 3D reconstructions of representative astrocytes from hippocampal sections obtained from mice administered with binge saline (CT) or Meth. Scale bar, 10 μm. (b) Sholl analysis of astrocytes (15–18 cells/group from $n = 3$ mice per group. Data were analyzed by two-way analysis of variance (ANOVA) corrected for multiple comparisons using the Bonferroni multiple comparison post hoc test, $^{****}p < .0001$, $^{***}p < .001$, $^{**}p < .01$, or $^{*}p < .05$ when comparing the pMT-10 −Zn CT with pMT-10 −Zn Meth conditions, and #### $p < .0001$ or ## $p < .01$ when comparing pMT-10 −Zn Meth with pMT-10 +Zn Meth conditions. (c) Graph display (mean ± standard error of the mean) of Imaris-based automated quantification of astrocytic territorial area. Statistical analysis was conducted using one-way ANOVA ($^{*}p < .05$; $^{****}p < .0001$ and ns, non-significant).

Cdc42 Meth-induced activation is either downstream of Ca^{2+} release, or Ca^{2+}-independent.

3.5 | In vivo IL-10 prevents Meth-induced neuroinflammation and compromised risk assessment

To investigate the protective role of IL-10 in an in vivo model of Meth administration, we used a transgenic mouse model of IL-10 overexpression under the control of the metallothionein promoter, designated pMT-10 mouse (Cardoso et al., 2018). IL-10 expression in these mice reaches detectable concentrations in the serum as early as 3 days following zinc (Zn) sulfate administration in the drinking water, a regimen previously established (Cardoso et al., 2018). These levels are furthermore comparable to IL-10 levels observed in IL-10-treated humans (Huhn et al., 1996; Huhn et al., 1997).

pMT-10 animals were exposed to Zn for 3 consecutive days, followed by Meth administration (Figure S3A). Considering the substantial decrease in IL-10 levels seen upon cessation of Zn administration (Cardoso et al., 2018), Zn treatment (and control water) was continued during the Meth administration period.

We have demonstrated that increased levels of IL-10 in vitro prevent the effects of Meth in an astrocytic- and Cdc42 dependent way. Since Cdc42 was previously shown to influence astrocytic function and morphology (Robel et al., 2011), we investigated the impact of Meth and IL-10 in astrocyte morphology in vivo, using the pMT-10 mouse. Following Meth administration, we observed a notable alteration in astrocytes morphology, characterized by hypertrophy (Figure 4a), increased ramification (Figure 4b), and complexity (Figure 4c). Overexpression of IL-10 successfully prevented these changes in astrocytes, leading to a morphology comparable to control conditions (Figure 4a–c).

Our previous research has established that, in a mechanism mediated by astrocytes, acute Meth administration induces robust microgliosis and activation of a pro-inflammatory profile in WT mice (Canedo et al., 2021). Here, we found that elevating IL-10 levels

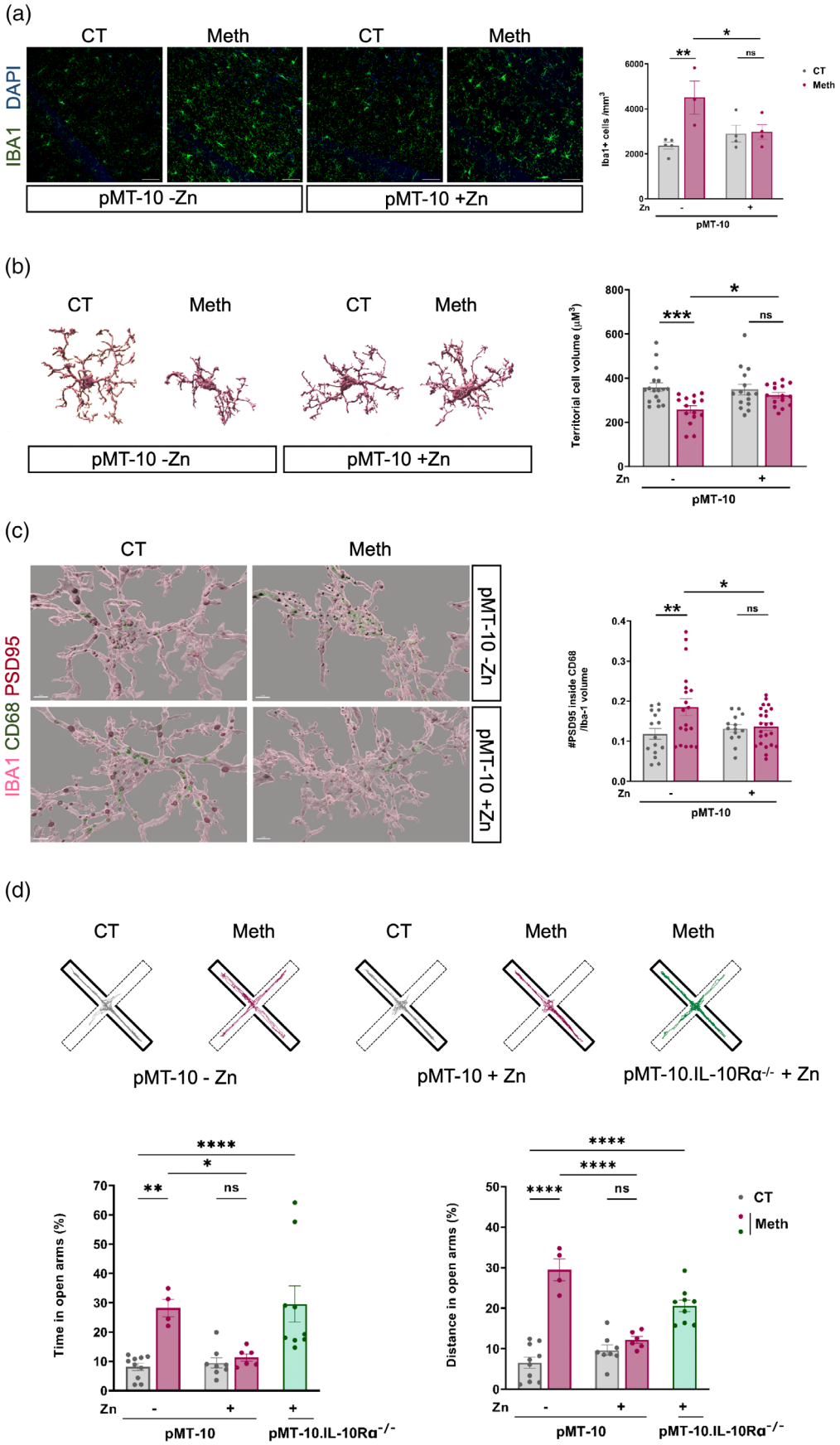

FIGURE 5 Legend on next page.

prevents the Meth-induced expansion of Iba1+ cells within the hippocampus (Figure 5a). Furthermore, the changes in microglial morphology induced by Meth and characterized by decreased territorial volume (Figure 5b) and less ramified shape (Figure S3B), were also mitigated by IL-10.

Microglial cells are pivotal in surveilling the brain and in pruning synapses (Paolicelli et al., 2011). To assess the impact of Meth administration on synapse elimination by microglia and the potential mitigating effects of IL-10, we analyzed the amount of PSD95 within microglial phagolysosomes. Meth administration resulted in significantly higher PSD95 puncta co-localizing in CD68+ structures of microglia cells compared to control, suggesting increased synapse elimination (Figure 5c). IL-10 effectively prevented these alterations (Figure 5c).

Meth is also known to impact behavior, including loss of risk assessment capacity (Canedo et al., 2021). To evaluate this, pMT-10 mice exposed to Meth were tested in the EPM, a well-established paradigm for evaluating anxiety-like behaviors (Walf & Frye, 2007). After Meth administration, mice exhibited a significant increase in the time and distance traveled within the open arms of the maze (Figure 5d), indicating compromised risk assessment. Notably, IL-10 prevented these behavioral changes (Figure 5d). Of note, the effects of Zn administration on pMT-10 mice were mediated by IL-10, as in pMT-10 mice lacking a functional IL-10 receptor (pMT10.IL-10Rα$^{-/-}$), the protective effect of IL-10 over Meth-induced behavior alterations, was no longer observed (Figure 5d).

Collectively, these findings underscore the protective role of IL-10 in mitigating Meth-induced neuroinflammation and behavioral alterations, highlighting its potential therapeutic significance in the context of substance abuse.

4 | DISCUSSION

Growing evidence suggests that neuroinflammation plays a pivotal role in Meth's pathophysiology (Shi et al., 2022). Several authors have shown that Meth exposure induces astrocytic reactivity (Dang et al., 2021; Escartin et al., 2021), which is closely linked to increased neurotoxicity and neuroinflammation, both in vitro (Bortell et al., 2017) and in vivo (Narita et al., 2006). In humans, Meth use leads to microglia activation (Sekine et al., 2008). However, as we have previously reported, Meth does not induce a pro-inflammatory state in primary microglia in a cell-autonomous way, requiring an astrocytes-to-microglia crosstalk (Canedo et al., 2021). Here, we show that the anti-inflammatory cytokine IL-10 prevents Meth-induced microglia activation by acting on astrocytes. Our current findings highlight that Meth-induced glutamate release is mediated by Ca^{2+} and Cdc42 activation. Importantly, we have demonstrated that the protective effect of IL-10 is also manifested through its action on Cdc42, preventing glutamate release. This new insight not only improves our understanding of the intricate mechanisms underlying Meth-action but also emphasizes the prospective therapeutic relevance of IL-10 in modulating these pathways. The present results successfully demonstrate that elevated levels of IL-10 in animals exposed to Meth can play a crucial role in preventing microglial activation. This significant finding suggests a potential therapeutic avenue, as manipulating IL-10 levels could offer a strategy to mitigate the adverse effects of Meth exposure on microglia activation.

We have demonstrated that the presence of IL-10 in astrocyte cultures exposed to Meth effectively reduced microglial activation, evidenced by decreased CD68 and iNOS markers. Concurrently, direct IL-10 addition to microglia showed no discernible effect. These findings align with previous reports where transgenic IL-10 production by astrocytes downregulated microglial activation after injury (Recasens et al., 2019). Of note, this notion of astrocyte-mediated IL-10-attenuation of microglia activation, seems to be supported by a higher abundance of IL-10 receptors in astrocytes, compared to microglia, that makes them more sensitive to IL-10 (Norden et al., 2014; Recasens et al., 2019).

Our previous research indicated that Meth-induced microglial activation is linked to increased glutamate release, as blocking glutamate receptors in microglia prevented their activation (Canedo et al., 2021). Thus, we hypothesized that the protective effect of IL-10 may operate by inhibiting this glutamate release. Employing FRET analysis, we observed in real-time that IL-10 mitigated Meth-triggered astrocytic glutamate release, underscoring IL-10's role as a modulator of astrocyte-mediated glutamate release (Figure 6b). The protective role of IL-10 over glutamate toxicity has been previously described, IL-10 prevented glutamate-mediated cell death (Bachis et al., 2001), and protected neurons against glutamate-induced excitotoxicity by normalizing intracellular Ca^{2+} levels through the PI3K-AKT pathway (Sharma et al., 2011; Tukhovskaya et al., 2014; Turovskaya et al., 2012), which

FIGURE 5 IL-10 prevents Meth-induced neuroinflammation and loss of risk-assessment in the pMT-10 mouse. (a) Representative confocal imaging of hippocampal sections from pMT-10 mice administered with binge saline (CT) or Meth and immunostained for Iba1 (green) and DAPI (magenta). Scale bar, 50 μm. Graph displays (mean ± standard error of the mean[SEM]) the number of Iba1+ cells per mm^3 (9 sections/animal from $N = 3$–5 mice per group). Statistical analysis was conducted using one-way analysis of variance (ANOVA) (**$p < .01$ and ns, non-significant). (b) Imaris (Bitplane)-based 3D reconstructions of representative microglia from hippocampal sections obtained from mice administered with binge saline (CT) or Meth. Graph displays (mean ± SEM) of Imaris-based automated quantification of microglial territorial cell volume ($n = 15$–18 cells/group from $N = 3$ mice per group). Statistical analysis was conducted using one-way ANOVA (***$p < .001$ and ns, non-significant). (c) Representative 3D surface rendering showing volume reconstruction of Iba1+ (magenta), CD68 (green), and PSD95 (red). Scale bar, 7 μm. The graph displays (mean ± SEM) relative quantification of engulfed PSD95 within CD68 per microglia ($n = 14$–23 cells/group from $N = 3$ mice per group). Statistical analysis was conducted using one-way ANOVA (**$p < .01$ and ns, non-significant). (d) Animals were evaluated in the EPM 24 h after binge saline (CT) or Meth. Graphs represent mean ± SEM for CT and Meth-treated mice, displayed significant differences in time spent in open arms and distance traveled in open arms ($n = 4$–10 animals per group). Statistical analysis was conducted using one-way ANOVA, (*$p < .05$, **$p < .01$, ***$p < .001$, ****$p < .0001$ and ns, non-significant).

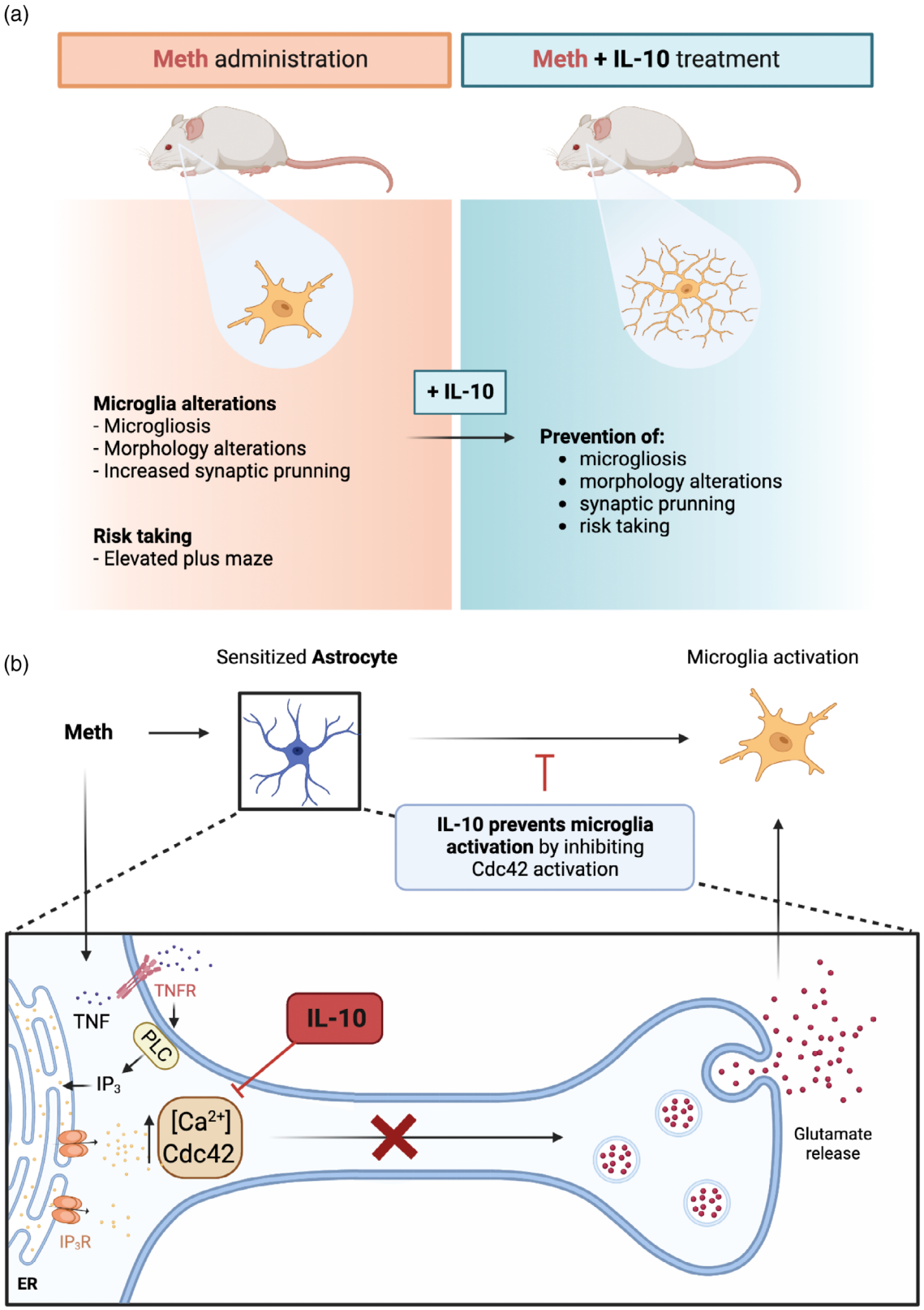

FIGURE 6 IL-10 prevents microgliosis and behavior impairment by inhibiting Cdc42. (a) Meth exposure causes microgliosis, altered microglia morphology and increased synaptic pruning. Meth also alters animal behavior, impairing risk-assessment. IL-10 prevents these Meth-induced effects. Created with BioRender.com. (b) In astrocytes Meth exposure triggers Ca^{2+} mobilization from the ER into the cytosol, leading to an elevation in intracellular Ca^{2+} levels. Consequently, this heightened Ca^{2+} concentration promotes the release of glutamate into the extracellular milieu, promoting the activation of microglia cells. IL-10 exerts its regulatory influence by inhibiting both Ca^{2+} efflux and Cdc42 activity in astrocytes and consequently, preventing the release of glutamate and activation of microglia cells. Created with BioRender.com.

fits with our results showing that, in astrocytes, IL-10 can prevent Meth-induced glutamate release in a Ca^{2+}-dependent manner.

Our investigation into the interplay between IL-10, Rho GTPases, and Ca^{2+} signaling has unveiled novel insights into the pathways triggered by Meth in astrocytes. Rho GTPases, including RhoA, Rac1, and Cdc42, regulate various cellular processes, including cytoskeletal dynamics and vesicle trafficking (Heasman & Ridley, 2008), and extending to the modulation of intracellular Ca^{2+} levels (Jin et al., 2005). In our hands, Cdc42 emerged as a critical player in Meth-induced astrocytic glutamate release. Meth led to a rapid and sustained elevation in Cdc42 activity, which IL-10 effectively prevented. This was concurrent with a significant decrease in glutamate release. Using the Cdc42 inhibitor Zcl278, we confirmed the crucial role of Cdc42 in these processes. Despite its considerable impact on glutamate exocytosis, the partial reduction of ER Ca^{2+} release upon Cdc42 inhibition suggests that Cdc42 contributes to glutamate release but does not solely determine Ca^{2+} dynamics. This highlights the need for further studies to establish causative relationships. Additionally, our study revealed that Meth exposure alone did not significantly affect c-Src activity in astrocytes. Thus, the reduction in Ca^{2+} release from the ER following IL-10 treatment suggests that IL-10's influence may occur through alternative pathways (Figure 6b).

These in vitro findings are further supported by evidence demonstrating that the in vivo protective effects of IL-10 in Meth-exposure may be mediated through astrocytes. Elevated IL-10 levels appear to effectively counteract Meth-induced changes in astrocyte morphology that are associated to reactive astrogliosis (Escartin et al., 2021). Using the IP3R2 KO mouse, we have previously demonstrated that astrocytic-Ca^{2+} release mediates Meth-induced changes in microglia and anxiety-like behavior (Canedo et al., 2021). Corroborating our in vitro data, here, we further show that the IL-10 protective effect in vivo, importantly reduces Meth-induced reactivity in astrocytes.

IL-10 has previously been recognized for its significance in brain disorders such as depression (Mesquita et al., 2008). Here, using a transgenic mouse model that enabled us to modulate IL-10 levels in a time-controlled manner, we highlighted the crucial role of IL-10 in mitigating in vivo Meth-induced microglial alterations, including microgliosis, changes in microglial morphology, and increased synaptic pruning by microglia. IL-10, also counteracted the Meth-induced changes observed in the EPM, preventing the behaviors associated with decreased anxiety-like levels and impaired risk assessment (Figure 6a). Together with previous reports showing that overexpressing IL-10 could decrease opioid self-administration in rats (Lacagnina et al., 2017), or that rIL-10 attenuated ethanol consumption in mice (Marshall et al., 2017), the present results evidence the promising therapeutical potential of IL-10 in drug associated disorders. Importantly, our results add relevant mechanistical detail into IL-10 action, confirming its role in Ca^{2+}-mediated glutamate release, and revealing Cdc42 as another interesting therapeutical target in drug related disorders.

AUTHOR CONTRIBUTIONS

Conceptualization: A.I.S, R.S., J.B.R., M.S., and T.S.; investigation: A.I.S, C.P., T.C. and A.F.T.; formal analysis: A.I.S., M.S. and T.S.; writing—original draft: A.I.S, R.S., M.S. and T.S.; writing—review and editing: all authors; resources: T.S.; funding acquisition: T.S.; supervision and project administration: T.S., M.S., J.B.R.

ACKNOWLEDGMENTS

This work was funded by National Funds through FCT—Fundação para a Ciência e a Tecnologia, I.P., under the project PTDC/SAU-TOX/0067/2021 in Summavielle's lab, this project has also supported the work of TC. AIS and AFT were supported by FCT (SFRH/BD/144324/2019, 2020.07188.BD). RS holds employment contracts financed by national funds through FCT–in the context of the program-contract described in paragraphs 4, 5, and 6 of art. 23 of Law no. 57/ 2016, of August 29, as amended by Law no. 57/2017 of July 2019. TS and MS are funded by FCT through 2022.03699.CEECIND and CEECIND/00241/2017, respectively. We acknowledge the support of the following i3S Scientific Platforms: BioSciences Screening, member of the PT-OPENSCREEN (NORTE-01-0145-FEDER-085468) and advanced light microscopy (ALM), a member of the national infrastructure PPBI-Portuguese Platform of BioImaging (supported by POCI-01-0145-FEDER-022122), and animal facility, and we thank André Maia, António Pombinho, Maria Azevedo, and Sofia Lamas from these facilities for their technical support.

CONFLICT OF INTEREST STATEMENT

The authors of the submitted paper entitled: "IL-10 and Cdc42 modulate astrocyte-mediated microglia activation in methamphetamine-induced neuroinflammation," Ana Isabel Silva, Renato Socodato, Carolina Pinto, Ana Filipa Terceiro, Teresa Canedo, João Bettencourt Relvas, Margarida Saraiva, Teresa Summavielle declare that the research was conducted in the absence of any commercial or financial relationships that could be construed as a potential conflict of interest.

DATA AVAILABILITY STATEMENT

The data that support the findings of this study are available from the corresponding author upon reasonable request.

ORCID

Ana Isabel Silva https://orcid.org/0000-0002-9434-516X
Renato Socodato https://orcid.org/0000-0002-6882-5020
Carolina Pinto https://orcid.org/0000-0001-5844-5078
Ana Filipa Terceiro https://orcid.org/0000-0001-7569-2732
Teresa Canedo https://orcid.org/0000-0002-4000-153X
João Bettencourt Relvas https://orcid.org/0000-0001-7636-0924
Margarida Saraiva https://orcid.org/0000-0002-8180-1293
Teresa Summavielle https://orcid.org/0000-0003-2548-6281

REFERENCES

Allen, N. J., Bennett, M. L., Foo, L. C., Wang, G. X., Chakraborty, C., Smith, S. J., & Barres, B. A. (2012). Astrocyte glypicans 4 and 6 promote formation of excitatory synapses via GluA1 AMPA receptors. *Nature*, *486*(7403), 410–414. https://doi.org/10.1038/nature11059

Althammer, F., Ferreira-Neto, H. C., Rubaharan, M., Roy, R. K., Patel, A. A., Murphy, A., Stern, J. E., & Stern, J. E. (2020). Three-dimensional morphometric analysis reveals time-dependent structural changes in microglia and astrocytes in the central amygdala and hypothalamic paraventricular nucleus of heart failure rats.

Journal of Neuroinflammation, *17*(1), 221. https://doi.org/10.1186/s12974-020-01892-4

An, Y., Liu, T., Liu, X., Zhao, L., & Wang, J. (2016). Rac1 and Cdc42 play important roles in arsenic neurotoxicity in primary cultured rat cerebellar astrocytes. *Biological Trace Element Research*, *170*(1), 173–182. https://doi.org/10.1007/s12011-015-0456-7

Anguita, E., & Villalobo, A. (2017). Src-family tyrosine kinases and the Ca(2+) signal. *Biochimica et Biophysica Acta (BBA)—Molecular Cell Research*, *1864*(6), 915–932. https://doi.org/10.1016/j.bbamcr.2016.10.022

Aspenström, P. (2004). Integration of signalling pathways regulated by small GTPases and calcium. *Biochimica et Biophysica Acta*, *1742*(1–3), 51–58. https://doi.org/10.1016/j.bbamcr.2004.09.029

Bachis, A., Colangelo, A. M., Vicini, S., Doe, P. P., De Bernardi, M. A., Brooker, G., & Mocchetti, I. (2001). Interleukin-10 prevents glutamate-mediated cerebellar granule cell death by blocking caspase-3-like activity. *The Journal of Neuroscience*, *21*(9), 3104–3112. https://doi.org/10.1523/jneurosci.21-09-03104.2001

Bortell, N., Basova, L., Semenova, S., Fox, H. S., Ravasi, T., & Marcondes, M. C. (2017). Astrocyte-specific overexpressed gene signatures in response to methamphetamine exposure in vitro. *Journal of Neuroinflammation*, *14*(1), 49. https://doi.org/10.1186/s12974-017-0825-6

Burmeister, A. R., & Marriott, I. (2018). The Interleukin-10 family of cytokines and their role in the CNS. *Frontiers in Cellular Neuroscience*, *12*, 458. https://doi.org/10.3389/fncel.2018.00458

Canedo, T., Portugal, C. C., Socodato, R., Almeida, T. O., Terceiro, A. F., Bravo, J., Silva, A. I., Magalhães, J. D., Guerra-Gomes, S., Oliveira, J. F., Sousa, N., Magalhães, A., Relvas, J. B., & Summavielle, T. (2021). Astrocyte-derived TNF and glutamate critically modulate microglia activation by methamphetamine. *Neuropsychopharmacology*, *46*(13), 2358–2370. https://doi.org/10.1038/s41386-021-01139-7

Cardoso, A., Gil Castro, A., Martins, A. C., Carriche, G. M., Murigneux, V., Castro, I., Cumano, A., Vieira, P., & Saraiva, M. (2018). The dynamics of Interleukin-10-afforded protection during dextran sulfate sodium-induced colitis. *Frontiers in Immunology*, *9*, 400. https://doi.org/10.3389/fimmu.2018.00400

Cardoso, A., Martins, A. C., Maceiras, A. R., Liu, W., Castro, I., Castro, A. G., Bandeira, A., di Santo, J. P., Cumano, A., Li, Y., Vieira, P., & Saraiva, M. (2021). Interleukin-10 induces interferon-γ-dependent emergency myelopoiesis. *Cell Reports*, *37*(4), 109887. https://doi.org/10.1016/j.celrep.2021.109887

Costello, P. S., Walters, A. E., Mee, P. J., Turner, M., Reynolds, L. F., Prisco, A., Sarner, N., Zamoyska, R., & Tybulewicz, V. L. (1999). The rho-family GTP exchange factor Vav is a critical transducer of T cell receptor signals to the calcium, ERK, and NF-kappaB pathways. *Proceedings of the National Academy of Sciences of the United States of America*, *96*(6), 3035–3040. https://doi.org/10.1073/pnas.96.6.3035

Courtney, K. E., & Ray, L. A. (2014). Methamphetamine: An update on epidemiology, pharmacology, clinical phenomenology, and treatment literature. *Drug and Alcohol Dependence*, *143*, 11–21. https://doi.org/10.1016/j.drugalcdep.2014.08.003

Dang, J., Tiwari, S. K., Agrawal, K., Hui, H., Qin, Y., & Rana, T. M. (2021). Glial cell diversity and methamphetamine-induced neuroinflammation in human cerebral organoids. *Molecular Psychiatry*, *26*(4), 1194–1207. https://doi.org/10.1038/s41380-020-0676-x

de Vellis, J., & Cole, R. (2012). Preparation of mixed glial cultures from postnatal rat brain. *Methods in Molecular Biology*, *814*, 49–59. https://doi.org/10.1007/978-1-61779-452-0_4

Ding, J., Huang, J., Tang, X., Shen, L., Hu, S., He, J., Liu, T., Yu, Z., Liu, Y., Wang, Q., Wang, J., Zhao, N., Qi, X., & Huang, J. (2022). Low and high dose methamphetamine differentially regulate synaptic structural plasticity in cortex and hippocampus. *Frontiers in Cellular Neuroscience*, *16*, 1003617. https://doi.org/10.3389/fncel.2022.1003617

Djouder, N., Prepens, U., Aktories, K., & Cavalie, A. (2000). Inhibition of calcium release-activated calcium current by Rac/Cdc42-inactivating clostridial cytotoxins in RBL cells. *The Journal of Biological Chemistry*, *275*(25), 18732–18738. https://doi.org/10.1074/jbc.M001425200

Escartin, C., Galea, E., Lakatos, A., O'Callaghan, J. P., Petzold, G. C., Serrano-Pozo, A., Steinhäuser, C., Volterra, A., Carmignoto, G., Agarwal, A., Allen, N. J., Araque, A., Barbeito, L., Barzilai, A., Bergles, D. E., Bonvento, G., Butt, A. M., Chen, W. T., Cohen-Salmon, M., … Verkhratsky, A. (2021). Reactive astrocyte nomenclature, definitions, and future directions. *Nature Neuroscience*, *24*(3), 312–325. https://doi.org/10.1038/s41593-020-00783-4

Farina, C., Aloisi, F., & Meinl, E. (2007). Astrocytes are active players in cerebral innate immunity. *Trends in Immunology*, *28*(3), 138–145. https://doi.org/10.1016/j.it.2007.01.005

Friesland, A., Zhao, Y., Chen, Y. H., Wang, L., Zhou, H., & Lu, Q. (2013). Small molecule targeting Cdc42-intersectin interaction disrupts Golgi organization and suppresses cell motility. *Proceedings of the National Academy of Sciences of the United States of America*, *110*(4), 1261–1266. https://doi.org/10.1073/pnas.1116051110

Giusti, A. F., Carroll, D. J., Abassi, Y. A., Terasaki, M., Foltz, K. R., & Jaffe, L. A. (1999). Requirement of a Src family kinase for initiating calcium release at fertilization in starfish eggs. *The Journal of Biological Chemistry*, *274*(41), 29318–29322. https://doi.org/10.1074/jbc.274.41.29318

Harada, K., Kamiya, T., & Tsuboi, T. (2015). Gliotransmitter release from astrocytes: Functional, developmental, and pathological implications in the brain. *Frontiers in Neuroscience*, *9*, 499s. https://doi.org/10.3389/fnins.2015.00499

Heasman, S. J., & Ridley, A. J. (2008). Mammalian rho GTPases: New insights into their functions from in vivo studies. *Nature Reviews. Molecular Cell Biology*, *9*(9), 690–701. https://doi.org/10.1038/nrm2476

Hong-Geller, E., & Cerione, R. A. (2000). Cdc42 and Rac stimulate exocytosis of secretory granules by activating the IP(3)/calcium pathway in RBL-2H3 mast cells. *The Journal of Cell Biology*, *148*(3), 481–494. https://doi.org/10.1083/jcb.148.3.481

Huhn, R. D., Radwanski, E., Gallo, J., Affrime, M. B., Sabo, R., Gonyo, G., Monge, A., & Cutler, D. L. (1997). Pharmacodynamics of subcutaneous recombinant human interleukin-10 in healthy volunteers. *Clinical Pharmacology and Therapeutics*, *62*(2), 171–180. https://doi.org/10.1016/s0009-9236(97)90065-5

Huhn, R. D., Radwanski, E., O'Connell, S. M., Sturgill, M. G., Clarke, L., Cody, R. P., Affrime, M. B., & Cutler, D. L. (1996). Pharmacokinetics and immunomodulatory properties of intravenously administered recombinant human interleukin-10 in healthy volunteers. *Blood*, *87*(2), 699–705.

Inaba, H., Miao, Q., & Nakata, T. (2021). Optogenetic control of small GTPases reveals RhoA mediates intracellular calcium signaling. *The Journal of Biological Chemistry*, *296*, 100290. https://doi.org/10.1016/j.jbc.2021.100290

Jin, M., Guan, C. B., Jiang, Y. A., Chen, G., Zhao, C. T., Cui, K., Song, Y. Q., Wu, C. P., Poo, M. M., & Yuan, X. B. (2005). Ca2+−dependent regulation of rho GTPases triggers turning of nerve growth cones. *The Journal of Neuroscience*, *25*(9), 2338–2347. https://doi.org/10.1523/jneurosci.4889-04.2005

Lacagnina, M. J., Kopec, A. M., Cox, S. S., Hanamsagar, R., Wells, C., Slade, S., Grace, P. M., Watkins, L. R., Levin, E. D., & Bilbo, S. D. (2017). Opioid self-administration is attenuated by early-life experience and gene therapy for anti-inflammatory IL-10 in the nucleus Accumbens of male rats. *Neuropsychopharmacology*, *42*(11), 2128–2140. https://doi.org/10.1038/npp.2017.82

Lim, S. H., Park, E., You, B., Jung, Y., Park, A. R., Park, S. G., & Lee, J. R. (2013). Neuronal synapse formation induced by microglia and interleukin 10. *PLoS One*, *8*(11), e81218. https://doi.org/10.1371/journal.pone.0081218

Limanaqi, F., Gambardella, S., Biagioni, F., Busceti, C. L., & Fornai, F. (2018). Epigenetic effects induced by methamphetamine and methamphetamine-dependent oxidative stress. *Oxidative Medicine and Cellular Longevity*, *2018*, 4982453. https://doi.org/10.1155/2018/4982453

Liu, X., Gao, Y., An, Y., Fu, X., Li, Y., Sun, D., & Wang, J. (2015). Neuroglobin plays a protective role in Arsenite-induced cytotoxicity by inhibition of Cdc42 and Rac1GTPases in rat cerebellar granule neurons. *Cellular Physiology and Biochemistry*, *36*(4), 1613–1627. https://doi.org/10.1159/000430323

Lobo-Silva, D., Carriche, G. M., Castro, A. G., Roque, S., & Saraiva, M. (2016). Balancing the immune response in the brain: IL-10 and its regulation. *Journal of Neuroinflammation*, *13*(1), 297. https://doi.org/10.1186/s12974-016-0763-8

Malarkey, E. B., & Parpura, V. (2008). Mechanisms of glutamate release from astrocytes. *Neurochemistry International*, *52*(1–2), 142–154. https://doi.org/10.1016/j.neuint.2007.06.005

Marshall, S. A., McKnight, K. H., Blose, A. K., Lysle, D. T., & Thiele, T. E. (2017). Modulation of binge-like ethanol consumption by IL-10 signaling in the basolateral amygdala. *Journal of Neuroimmune Pharmacology*, *12*(2), 249–259. https://doi.org/10.1007/s11481-016-9709-2

Mesquita, A. R., Correia-Neves, M., Roque, S., Castro, A. G., Vieira, P., Pedrosa, J., Palha, J. A., & Sousa, N. (2008). IL-10 modulates depressive-like behavior. *Journal of Psychiatric Research*, *43*(2), 89–97. https://doi.org/10.1016/j.jpsychires.2008.02.004

Minuz, P., Meneguzzi, A., Fumagalli, L., Degan, M., Calabria, S., Ferraro, R., Ricci, M., Veneri, D., & Berton, G. (2018). Calcium-dependent Src phosphorylation and reactive oxygen species generation are implicated in the activation of human platelet induced by thromboxane A2 analogs. *Frontiers in Pharmacology*, *9*, 1081. https://doi.org/10.3389/fphar.2018.01081

Narita, M., Miyatake, M., Narita, M., Shibasaki, M., Shindo, K., Nakamura, A., Kuzumaki, N., Nagumo, Y., & Suzuki, T. (2006). Direct evidence of astrocytic modulation in the development of rewarding effects induced by drugs of abuse. *Neuropsychopharmacology*, *31*(11), 2476–2488. https://doi.org/10.1038/sj.npp.1301007

Narita, M., Takagi, M., Aoki, K., Kuzumaki, N., & Suzuki, T. (2003). Implication of rho-associated kinase in the elevation of extracellular dopamine levels and its related behaviors induced by methamphetamine in rats. *Journal of Neurochemistry*, *86*(2), 273–282. https://doi.org/10.1046/j.1471-4159.2003.01784.x

Norden, D. M., Fenn, A. M., Dugan, A., & Godbout, J. P. (2014). TGFβ produced by IL-10 redirected astrocytes attenuates microglial activation. *Glia*, *62*(6), 881–895. https://doi.org/10.1002/glia.22647

Okumoto, S., Looger, L. L., Micheva, K. D., Reimer, R. J., Smith, S. J., & Frommer, W. B. (2005). Detection of glutamate release from neurons by genetically encoded surface-displayed FRET nanosensors. *Proceedings of the National Academy of Sciences of the United States of America*, *102*(24), 8740–8745. https://doi.org/10.1073/pnas.0503274102

Ouyang, M., Sun, J., Chien, S., & Wang, Y. (2008). Determination of hierarchical relationship of Src and Rac at subcellular locations with FRET biosensors. *Proceedings of the National Academy of Sciences of the United States of America*, *105*(38), 14353–14358. https://doi.org/10.1073/pnas.0807537105

Palmer, A. E., Jin, C., Reed, J. C., & Tsien, R. Y. (2004). Bcl-2-mediated alterations in endoplasmic reticulum Ca2+ analyzed with an improved genetically encoded fluorescent sensor. *Proceedings of the National Academy of Sciences of the United States of America*, *101*(50), 17404–17409. https://doi.org/10.1073/pnas.0408030101

Panenka, W. J., Procyshyn, R. M., Lecomte, T., MacEwan, G. W., Flynn, S. W., Honer, W. G., & Barr, A. M. (2013). Methamphetamine use: A comprehensive review of molecular, preclinical and clinical findings. *Drug and Alcohol Dependence*, *129*(3), 167–179. https://doi.org/10.1016/j.drugalcdep.2012.11.016

Paolicelli, R. C., Bolasco, G., Pagani, F., Maggi, L., Scianni, M., Panzanelli, P., Giustetto, M., Ferreira, T. A., Guiducci, E., Dumas, L., Ragozzino, D., & Gross, C. T. (2011). Synaptic pruning by microglia is necessary for normal brain development. *Science*, *333*(6048), 1456–1458. https://doi.org/10.1126/science.1202529

Pils, M. C., Pisano, F., Fasnacht, N., Heinrich, J. M., Groebe, L., Schippers, A., Rozell, B., Jack, R. S., & Müller, W. (2010). Monocytes/-macrophages and/or neutrophils are the target of IL-10 in the LPS endotoxemia model. *European Journal of Immunology*, *40*(2), 443–448. https://doi.org/10.1002/eji.200939592

Recasens, M., Shrivastava, K., Almolda, B., González, B., & Castellano, B. (2019). Astrocyte-targeted IL-10 production decreases proliferation and induces a downregulation of activated microglia/macrophages after PPT. *Glia*, *67*(4), 741–758. https://doi.org/10.1002/glia.23573

Robel, S., Bardehle, S., Lepier, A., Brakebusch, C., & Götz, M. (2011). Genetic deletion of cdc42 reveals a crucial role for astrocyte recruitment to the injury site in vitro and in vivo. *The Journal of Neuroscience*, *31*(35), 12471–12482. https://doi.org/10.1523/jneurosci.2696-11.2011

Ru, Q., Wang, Y., Zhou, E., Chen, L., & Wu, Y. (2023). The potential therapeutic roles of rho GTPases in substance dependence. *Frontiers in Molecular Neuroscience*, *16*, 1125277. https://doi.org/10.3389/fnmol.2023.1125277

Schafer, D. P., Lehrman, E. K., Heller, C. T., & Stevens, B. (2014). An engulfment assay: A protocol to assess interactions between CNS phagocytes and neurons. *Journal of Visualized Experiments*, (88), e51482. https://doi.org/10.3791/51482

Schwarz, J. M., Hutchinson, M. R., & Bilbo, S. D. (2011). Early-life experience decreases drug-induced reinstatement of morphine CPP in adulthood via microglial-specific epigenetic programming of anti-inflammatory IL-10 expression. *The Journal of Neuroscience*, *31*(49), 17835–17847. https://doi.org/10.1523/JNEUROSCI.3297-11.2011

Scofield, M. D., Boger, H. A., Smith, R. J., Li, H., Haydon, P. G., & Kalivas, P. W. (2015). Gq-DREADD selectively initiates glial glutamate release and inhibits Cue-induced cocaine seeking. *Biological Psychiatry*, *78*(7), 441–451. https://doi.org/10.1016/j.biopsych.2015.02.016

Sekine, Y., Ouchi, Y., Sugihara, G., Takei, N., Yoshikawa, E., Nakamura, K., Iwata, Y., Tsuchiya, K. J., Suda, S., Suzuki, K., Kawai, M., Takebayashi, K., Yamamoto, S., Matsuzaki, H., Ueki, T., Mori, N., Gold, M. S., & Cadet, J. L. (2008). Methamphetamine causes microglial activation in the brains of human abusers. *The Journal of Neuroscience*, *28*(22), 5756–5761. https://doi.org/10.1523/JNEUROSCI.1179-08.2008

Sharma, S., Yang, B., Xi, X., Grotta, J. C., Aronowski, J., & Savitz, S. I. (2011). IL-10 directly protects cortical neurons by activating PI-3 kinase and STAT-3 pathways. *Brain Research*, *1373*, 189–194. https://doi.org/10.1016/j.brainres.2010.11.096

SheikhBahaei, S., Morris, B., Collina, J., Anjum, S., Znati, S., Gamarra, J., Zhang, R., Gourine, A. V., & Smith, J. C. (2018). Morphometric analysis of astrocytes in brainstem respiratory regions. *The Journal of Comparative Neurology*, *526*(13), 2032–2047. https://doi.org/10.1002/cne.24472

Shi, S., Chen, T., & Zhao, M. (2022). The crosstalk between neurons and glia in methamphetamine-induced Neuroinflammation. *Neurochemical Research*, *47*(4), 872–884. https://doi.org/10.1007/s11064-021-03513-9

Socodato, R., Henriques, J. F., Portugal, C. C., Almeida, T. O., Tedim-Moreira, J., Alves, R. L., Canedo, T., Silva, C., Magalhães, A., Summavielle, T., & Relvas, J. B. (2020). Daily alcohol intake triggers aberrant synaptic pruning leading to synapse loss and anxiety-like behavior. *Science Signaling*, *13*(650), eaba5754. https://doi.org/10.1126/scisignal.aba5754

Socodato, R., Portugal, C. C., Domith, I., Oliveira, N. A., Coreixas, V. S., Loiola, E. C., Martins, T., Santiago, A. R., Paes-de-Carvalho, R., Ambrósio, A. F., & Relvas, J. B. (2015). c-Src function is necessary and sufficient for triggering microglial cell activation. *Glia*, *63*(3), 497–511. https://doi.org/10.1002/glia.22767

Socodato, R., Portugal, C. C., Rodrigues, A., Henriques, J., Rodrigues, C., Figueira, C., & Relvas, J. B. (2018). Redox tuning of Ca(2+) signaling in microglia drives glutamate release during hypoxia. *Free Radical Biology & Medicine*, *118*, 137–149. https://doi.org/10.1016/j.freeradbiomed.2018.02.036

Swanepoel, T., Moller, M., & Harvey, B. H. (2018). N-acetyl cysteine reverses bio-behavioural changes induced by prenatal inflammation, adolescent methamphetamine exposure and combined challenges. *Psychopharmacology*, *235*(1), 351–368. https://doi.org/10.1007/s00213-017-4776-5

Tukhovskaya, E. A., Turovsky, E. A., Turovskaya, M. V., Levin, S. G., Murashev, A. N., Zinchenko, V. P., & Godukhin, O. V. (2014). Anti-inflammatory cytokine interleukin-10 increases resistance to brain ischemia through modulation of ischemia-induced intracellular Ca^{2+} response. *Neuroscience Letters*, *571*, 55–60. https://doi.org/10.1016/j.neulet.2014.04.046

Turovskaya, M. V., Turovsky, E. A., Zinchenko, V. P., Levin, S. G., & Godukhin, O. V. (2012). Interleukin-10 modulates [Ca2+]i response induced by repeated NMDA receptor activation with brief hypoxia through inhibition of InsP(3)-sensitive internal stores in hippocampal neurons. *Neuroscience Letters*, *516*(1), 151–155. https://doi.org/10.1016/j.neulet.2012.03.084

Tzschentke, T. M., & Schmidt, W. J. (2003). Glutamatergic mechanisms in addiction. *Molecular Psychiatry*, *8*(4), 373–382. https://doi.org/10.1038/sj.mp.4001269

Walf, A. A., & Frye, C. A. (2007). The use of the elevated plus maze as an assay of anxiety-related behavior in rodents. *Nature Protocols*, *2*(2), 322–328. https://doi.org/10.1038/nprot.2007.44

Wang, Y., Botvinick, E. L., Zhao, Y., Berns, M. W., Usami, S., Tsien, R. Y., & Chien, S. (2005). Visualizing the mechanical activation of Src. *Nature*, *434*(7036), 1040–1045. https://doi.org/10.1038/nature03469

Werry, E. L., Liu, G. J., Lovelace, M. D., Nagarajah, R., Hickie, I. B., & Bennett, M. R. (2011). Lipopolysaccharide-stimulated interleukin-10 release from neonatal spinal cord microglia is potentiated by glutamate. *Neuroscience*, *175*, 93–103. https://doi.org/10.1016/j.neuroscience.2010.10.080

Wheeler, M. A., Jaronen, M., Covacu, R., Zandee, S. E. J., Scalisi, G., Rothhammer, V., Tjon, E. C., Chao, C. C., Kenison, J. E., Blain, M., Rao, V. T. S., Hewson, P., Barroso, A., Gutiérrez-Vázquez, C., Prat, A., Antel, J. P., Hauser, R., & Quintana, F. J. (2019). Environmental control of astrocyte pathogenic activities in CNS inflammation. *Cell*, *176*(3), 581–596.e18. https://doi.org/10.1016/j.cell.2018.12.012

Xu, J., Dong, H., Qian, Q., Zhang, X., Wang, Y., Jin, W., & Qian, Y. (2017). Astrocyte-derived CCL2 participates in surgery-induced cognitive dysfunction and neuroinflammation via evoking microglia activation. *Behavioural Brain Research*, *332*, 145–153. https://doi.org/10.1016/j.bbr.2017.05.066

Xue, Y., He, J. T., Zhang, K. K., Chen, L. J., Wang, Q., & Xie, X. L. (2019). Methamphetamine reduces expressions of tight junction proteins, rearranges F-Actin cytoskeleton and increases the blood brain barrier permeability via the RhoA/ROCK-dependent pathway. *Biochemical and Biophysical Research Communications*, *509*(2), 395–401. https://doi.org/10.1016/j.bbrc.2018.12.144

Yang, X., Wang, Y., Li, Q., Zhong, Y., Chen, L., du, Y., He, J., Liao, L., Xiong, K., Yi, C. X., & Yan, J. (2018). The Main molecular mechanisms underlying methamphetamine- induced neurotoxicity and implications for pharmacological treatment. *Frontiers in Molecular Neuroscience*, *11*, 186. https://doi.org/10.3389/fnmol.2018.00186

Yoshizaki, H., Ohba, Y., Kurokawa, K., Itoh, R. E., Nakamura, T., Mochizuki, N., Nagashima, K., & Matsuda, M. (2003). Activity of rho-family GTPases during cell division as visualized with FRET-based probes. *The Journal of Cell Biology*, *162*(2), 223–232. https://doi.org/10.1083/jcb.200212049

SUPPORTING INFORMATION

Additional supporting information can be found online in the Supporting Information section at the end of this article.

How to cite this article: Silva, A. I., Socodato, R., Pinto, C., Terceiro, A. F., Canedo, T., Relvas, J. B., Saraiva, M., & Summavielle, T. (2024). IL-10 and Cdc42 modulate astrocyte-mediated microglia activation in methamphetamine-induced neuroinflammation. *Glia*, *72*(8), 1501–1517. https://doi.org/10.1002/glia.24542